Supporting Information

DnaN clamp zone provides a platform for spatiotemporal coupling of mismatch detection to DNA replication

Justin S. Lenhart, Anushi Sharma, Manju M. Hingorani, Lyle A. Simmons

SI Results

Mismatch detection by MutS is necessary for MutL-GFP focus formation. To further test the effects of the *mutSF30A* allele on MMR, we fused *mutL* to *gfp* to determine if the MutSF30A, which forms foci independent of mismatch binding, could elicit the downstream step of MutL-GFP focus formation. When native *mutS* is upstream of *mutL-gfp*, we found that ~16% of cells form MutL-GFP foci untreated (Fig S2). Challenge of MutL-GFP cells with 2-AP or placement into a genetic background containing a proofreading deficient $polC^{exo-}$ allele, we found an increase in the percent of cells with foci to ~36% and ~33% of cells respectively (Fig S2). This result shows that mismatches stimulate MutL to form foci *in vivo*. In contrast, a strain with a clean deletion of the *mutS* coding region showed a striking reduction in the percent of cells with MutL-GFP foci (<3% of cells) and in the absence of *mutS*, MutL-GFP foci were not stimulated by treatment with 2-AP (Fig S2). We asked if mismatch binding by MutS was required to elicit MutL-GFP foci. We show when *mutSF30A* replaces *mutS*, MutL-GFP foci formed in ~11% of cells. These foci were qualitatively dim relative to MutL-GFP foci that form in a $mutS^{+}$ strain. Furthermore, we found that in the *mutSF30A* strain, 2-AP failed to stimulate an increase in MutL-GFP focus formation when compared with wild type *mutS*. With these results we conclude that MutL-GFP focus formation is primarily driven by the formation of a binary complex between MutS and a mismatch, because *mutSF30A* is substantially reduced for MutL-GFP recruitment and unresponsive to 2-AP treatment (Fig S2).

MutL-GFP colocalizes with the replication apparatus. We also characterized the ability of MutL-mCherry to colocalize with the replisome. We constructed a strain with both *dnaX-gfp* and *mutL-mCherry* alleles, where both were integrated at their native locus and expressed from their native promoters. In exponentially growing cells, MutL-mCherry colocalized with the replisome at levels comparable to MutS (~59%, n=130) (Fig 3D). This result is different from results obtained in *S. cerevisiae*, where the Mlh1-PMS1 foci are not coincident with replication centers (Hombauer *et al.*, 2011). It should be noted however, that MutL foci in both organisms are dependent on MutS. When challenged with 2-AP, MutL-mCherry was reduced for colocalized with the replisome to ~49% (p=0.0568). Because MutL-GFP foci behave similarly to MutS-GFP foci when treated with 2-AP, we speculate that MutL may be poised with MutS at the replisome waiting for mismatch identification by MutS. We further speculate that upon the initiation of repair, MutL associates with the repair complex and moves away from the replisome in a complex that can be observed by fluorescence microscopy.

Experimental Procedures

MutS and MutSF30A protein purification

MutS and MutSF30A were overexpressed from pET11t-*mutS* and -*mutSF30A* respectively in *E. coli* $BL21_{DE3}$ using standard procedures (Klocko *et al.*, 2010). Cell pellets were resuspended in resuspension buffer (20 mM Tris HCl (pH 7.6), 500 mM NaCl, 4 mM DTT, 20 mM spermidine trihydrochloride, and 0.5 mM EDTA) and lysed by passage through a French pressure cell (3 passes at a setting of 15,000 PSI). Cells debris was pelleted at 15,000 rpm for 30 min at 4˚C. All subsequent protein purification steps were performed on ice or at 4˚C. Solid ammonium sulfate was added in order to achieve 30% saturation of the supernatant. Precipitated protein was removed by centrifugation at 15,000 rpm for 30 minutes. The supernatant was collected and

ammonium sulfate was added to 40% saturation, which preferentially precipitated MutS and MutSF30A. Precipitated protein was removed via centrifugation at 15,000 rpm for 30 min and flash frozen in liquid N_2 and stored at -80˚C.

The pellet was thawed on ice and then resuspended in buffer QA (20 mM Tris HCl (pH 7.6), 100 mM NaCl, 1 mM DTT, 0.5 mM EDTA, and 10% glycerol). Once the pellet was resuspended, the sample was desalted using HiPrep 26/10 desalting column (GE Healthcare, Uppsala, Sweden) pre-equilibrated in buffer QA. This material was further purified with a HiTrap Q HP column (GE Healthcare, Uppsala, Sweden) pre-equilibrated in Buffer QA. MutS and MutSF30A were eluted with a 20 column volume gradient (from 100 mM NaCl to 600 mM NaCl). MutS and MutSF30A containing fractions were pooled and once again desalted with a HiPrep 26/10 desalting column pre-equilibrated in Buffer HA1 (5 mM potassium phosphate (pH 7.4), 30 mM NaCl, 1 mM DTT, and 10% glycerol). The desalted sample was purified with a hydroxyapatite Bio-Scale Mini CHT Type 1 column (Bio-Rad) and eluted with a phosphate gradient (5 mM-400 mM) over 20 column volumes. Protein samples were concentrated with a Vivaspin 20 concentrator (GE Healthcare-28-9323-62) with a 50 kDa molecular weight cutoff and then desalted with a HiPrep 26/10 column using the following storage buffer (20 mM Tris HCl (pH 7.6), 200 mM NaCl, 4 mM DTT, and 10% glycerol). Samples were again concentrated with a Vivaspin 20 concentrator and aliquoted into small usable samples and flash frozen in liquid N_2. MutS and MutSF30A behaved identically throughout the purification process, indicating similar biochemical characteristics. Absorbance spectra were obtained using a 50-Bio UV Spectrophotometer (Varian, Palo Alto, CA) in both the natured state (storage buffer) and denatured state (storage buffer with 6M Guanidine HCl). No light scattering was observed from 300-600 nm in the native conditions, indicating the protein did not aggregate. In addition,

significant absorbance was not detected at 250 nm indicating nucleotides were not present. All protein concentrations were determined using extinction coefficients derived at ExPASy Proteomics Server (http://expasy.org/). DnaN was purified as described previously (Klocko *et al.*, 2011).

Construction of an unmarked-in frame *mutSF30A* mutant allele

In order to introduce the *mutSF30A* allele into the *B. subtilis* chromosome, we used the pMiniMAD2 vector as described (Patrick & Kearns, 2008). The pMiniMAD2 vector contains an erythromycin cassette, as well as a temperature sensitive origin of replication. Plasmid pJSL44 was introduced into PY79 via Campbell-type integration at the restrictive temperature (37˚C) for replication, selecting for integration of the plasmid into the chromosome by *mls* selection. After the initial Campbell type integration, pJSL44 was evicted as described (Patrick & Kearns, 2008). To rid the strain of the integrated plasmid, transformed colonies were grown in 3 ml of LB broth at a permissive temperature for plasmid replication (22°C) for 14 hr, diluted 30-fold in fresh LB broth and incubated at 22°C for another 8 hr. This process was continued over three successive days, and then serial dilutions were plated on LB agar at 37°C. Colonies were then colony purified on LB at the restrictive temperature and tested for *mls* resistance. Strains that were sensitive to *mls* selection were screened for increased spontaneous mutagenesis, consistent with a mismatch repair defect. The *mutS* gene was sequenced from clonal isolates showing a high increase in mutagenesis to verify the presence of the *F30A* change and to confirm that no other base changes were present.

Construction of an unmarked-in frame *ΔmutS* mutant allele

The *ΔmutS* allele was built in a similar way to the unmarked-in frame *mutSF30A* mutant allele. Differences are that a 500 bp region upstream of *mutS* was amplified with primers JSL 156/157 (insert A) and a 500 bp region downstream of *mutS* was amplified with pJSL 158/159 (insert B). Furthermore, we amplified the pMiniMAD2 vector (previously cut with KpnI in order to linearize the plasmid) with pJS282/283 to obtain a ~6.3 kB linear PCR product. These DNA fragments all maintained 20-25 bp of sequence homology between adjacently targeted segments. The two inserts, along with the prepared pMiniMAD2 vector were fused using sequence and ligation-independent cloning (SLIC) (Li & Elledge, 2007). The *ΔmutS* was integrated into the chromosome as described above for the *mutSF30A* mutant allele. The final strain was *ΔmutS,* as well as containing a deletion of the *mutSL* intergenic region. The resulting strain placed the 4-1881 bases of *mutL* fused with the start codon (bases 1-3) of *mutS*, as shown in SI Fig 4.

Thymidine incorporation to monitor DNA synthesis

B. subtilis cells were grown in $S7_{50}$ minimal media supplemented with 2% glucose at 37˚ C from an initial starting inoculum of 0.050. When the cells reached mid-exponential phase, 1.8 mL of culture was pulse labeled with 45 µL of ^{3}H-thymidine (50 Ci/mmol; 1 mCi/mL) and incubated at 37˚ C. At the appropriate time points (30, 120, 300 and 600s), 0.4 mL of culture were removed and mixed into 3 mL of ice cold 10% TCA and incubated on ice for ≥30 min. Samples were filtered on glass microfibre filters (GF/C, Whatman) by vacuum. Each filter was washed three times with 5 mL ice-cold 10% TCA, followed by three additional washes with 5 mL of -20˚C 70% ethanol. Filters were dried, and incorporated ^{3}H-thymidine into acid insoluble material during replication was was quantified using scintillation spectroscopy.

Plasmid construction

pJSL30 was constructed in order to place *mutS-gfp* expression under the control of the P_{spac} promoter at the ectopic *amyE* locus. The *mutS* gene was amplified from *B. subtilis* (PY79) chromosomal DNA using the primers oJSL81 and oJSL82. The insert was gel purified, digested with Sal I and Xho I, PCR purified, and ligated into pBS226 with the original *mutL* insert removed.

pJSL35 was constructed to knock out the mismatch detection capability of pJSL30 by introducing *mutSF30A*. To do so, pJSL30 was subject to site-directed mutagenesis using standard protocol (Zheng *et al.*, 2004) to produce the *F30A* mutation using the primers oJSL125 and oJSL126.

pJSL36 was constructed to generate the *mutSF30A* mutant allele at the native locus by allelic replacement (Patrick & Kearns, 2008). The sequence spanning from 457 bases upstream of the *mutS* +1 base to 570 bases downstream was PCR amplified from the *B. subtilis* PY79 chromosomal DNA using the primers oJSL123 and oJSL124. The fragment was gel extracted, digested with Bam HI and Kpn I, and ligated into pMiniMAD2. pMiniMAD2 contains an erythromycin cassette, as well as a temperature sensitive origin of replication (37˚).

pJSL40 was constructed to place codon optimized (C.o.) and monomeric CFP downstream of *dnaX* for native locus integration. *C.o. cfp* was amplified from pDR200 (Doan *et al.*, 2005) with primers oJSL127 and oJSL128. The fragment was gel purified, cut with restriction enzymes Sph I and Xho I, and ligated into pKL147 with the *gfp* insert removed.

pJSL44 was constructed to knock out the mismatch detection capability of MutS at its native locus. pJSL44 is pJSL36 with the *F30A* mutation introduced by site-directed mutagenesis

(Zheng et al., 2004). The primers used for site-directed mutagenesis reaction oJSL125 and oJSL126.

pJSL45 was constructed to overexpress wild type recombinant MutSF30A. The *F30A* was introduced into *pET11t-mutS* using primers oJSL125 and oJSL126.

pJSL57 (See supplemental methods)

pJSL58 was constructed to place *mutS800* under the control of a P_{spac} promoter at the *amyE* ectopic locus. The *mutS800* allele was PCR amplified from the *B. subtilis* chromosome using primers oJSL178 and oJSL179. We gel purified and digested the PCR fragment with SphI and NheI, followed by a PCR clean-up step (Qiagen). Finally, the digested fragment was ligated into pDR110 following digestion with the same restriction enzymes.

pJSL63 was constructed to place *mutS800-gfp* under the control of the P_{spac} promoter at the *amyE* ectopic locus. The *mutS800* allele was PCR amplified from the *B. subtilis* chromosome using primers oJSL81 and oJSL133. The PCR product was digested with Xho I and Sal I followed by gel purification. This digested fragment was ligated into opened pBS226.

pJSL64 was constructed to place *mutSF30A800-gfp* under the control of the P_{spac} promoter at the *amyE* ectopic locus. This construct is derived from pJSL63, where the *F30A* was introduced by site-directed mutagenesis (Zheng et al., 2004) into the plasmid using primers oJSL125 and pJSL126.

pJSL67 was constructed for localizing DnaX within the cell using the mCherry fluorophore. The *dnaX-mCherry* was PCR amplified from pJSL52 (*pKL147-dnaX-mCherry*)

using primers oJSL170 and 171. Using SLIC (see methods), the insert was ligated into pBGSC6 that was amplified using primers JSL168 and oJSL169.

All constructs were sequenced prior to use (University of Michigan core sequencing facility).

Table S1. Functional characterization of fusion alleles used within this study

Relevant genotype	No. of cultures	Mutation rate (10^{-9} mutations/generation)± [95% CI]	Relative mutation rate (% MMR activity)[a]
PY79 (wild type)*	51	1.82 [1.14-2.37]	1 (100%)
*mutSL::spec**	23	154.4 [146.6-162.2]	84.9 (0%)
mutL::mutL-GFP (spc)	25	139.8 [130.7-148.8]	76.9 (9.5%)
mutS::mutS-GFP (spec), amyE::P_{spac}-mutL (cm)	23	17.0 [12.5-21.5]	9.4 (89.0%)
mutS::mutS-YFP (cm) , amyE::P_{spac}-mutL (mls), dnaX::dnaX-coCFP (spc)	23	15.2 [10.5-19.9]	8.4 (90.2%)
ΔmutS, amyE:P_{spac} mutS (kan)	25	3.09 [1.35-4.68]	1 (100%)
ΔmutS, amyE:P_{spac} mutS-GFP (cm)	23	20.8 [16.0-25.6]	6.7 (88.7%)
ΔmutS, amyE:P_{spac} mutS800-GFP (cm)	30	133.3 [125.7-140.9]	43.1 (16.6%)
ΔmutS, amyE:P_{spac} mutS800-GFP (cm), dnaX::dnaX-mCherry (spc)	19	127.5 [120.8-134.2]	41.3 (20.2%)

* Data also found within Table 1.

[#] Calculations based on data obtained in Table 2 using isogenic *ΔmutS* backgrounds (JSL292 and JSL281). Brackets enclose the lower bounds and upper bounds of the 95% confidence limits

[a] % MMR activity was determined using the following equation: [(R.M.R.null - R.M.R.strain)/(R.M.R.null-R.M.R.wild-type)]•100. The designation "co" represents the codon optimized version of CFP (Doan et al., 2005).

Table S2. *Bacillus subtilis* strains used in this study

Strain	Relevant Genotype	Source or reference
JSL1	PY79-Prototroph, SPβ˚	(Youngman *et al.*, 1984)
LAS45	*mutS::mutS800-gfpmut2 (spc), amyE::Ps$_{pac}$-mutL (cm)*	(Simmons *et al.*, 2008)
LAS86	*mutS::mutS800 (spc), amyE::P$_{spac}$-mutL (cm*	(Simmons et al., 2008)
LAS440	*mutS::mutS-gfpmut2 (spc), amyE::P$_{spac}$-mutL (cm)*	(Smith *et al.*, 2001)
LAS397	*mutL::mutL-gfp (spc)*	(Smith et al., 2001)
LAS392	*amyE::P$_{spac}$-mutS-mgfpmut2 (cm)*	(Simmons et al., 2008)
NMD11	*dnaN5(G73R), spoIIIJ::kan*	(Dupes *et al.*, 2010)
JSL171	*amyE::P$_{spac}$-mutS-mgfpmut2 (cm)*	
JSL196	*amyE::P$_{spac}$-mutSF30A-mgfpmut2 (cm)*	
JSL201	*mut-1[polC G430E, S621N] (cm), mutL::mutL-gfpmut2(spc)*	This work and (Sanjanwala & Ganesan, 1991)
JSL202	*mut-1[polC G430E, S621N] (cm), mutS::mutS-mgfpmut2 (spc), amyE::P$_{spac}$-mutL (mls)*	
JSL204	*mutSF30A*	
JSL214	*mutSL::spec, amyE::P$_{spac}$-mutSF30A-gfpmut2 (cm)*	
JSL217	*mutS::mutSF30A-mgfpmut2 (spc), amyE::P$_{spac}$-mutL (mls)*	
JSL219	*mutSL::spc, amyE::P$_{spac}$-mutS-F30A-gfpmut2 (cm)*	
JSL230	*mutSF30A::mutS-yfp (cm), amyE::P$_{spac}$-mutL (mls)*	
JSL234	*mutS::mutS-yfp (cm), amyE::P$_{spac}$-mutL (mls), dnaX::dnaX-CFP(opt)(spc)*	
BKM1725	*dnaX::dnaX-yfp (spc),pelB::Psoj (opt-rbs)-cfp(d)-spo0J (ΔparS) (cm)*	(Sullivan *et al.*, 2009)
JSL259	*dnaN5, SpoIIIJ::kan, mutSF30A::mutS-mGFPmut2, amyE::P$_{spac}$-mutL (mls)*	
JSL281	*ΔmutS*	
JSL292	*ΔmutS, amyE::P$_{spac}$-mutS(spc)*	

Table S2 continued

Strain	Relevant Genotype	Source or reference
JSL295	*ΔmutS, amyE::P_{spac}-mutS-gfp mut2(cm)*	
JSL297	*ΔmutS, amyE::P_{spac}-mutS800 (spc)*	
JSL297	*ΔmutS, amyE::P_{spac}-mutS800 (spc)*	
JSL298	*ΔmutS, amyE::P_{spac}-mutSF30A-gfpmut2 (cm)*	
JSL307	*ΔmutS, amyE::P_{spac}-mutS-gfpmut2 (cm), dnaX::dnaX-mCherry (spc)*	
JSL308	*mutL::mutL-gfpmut2 (spc), dnaX:dnaX-mCherry (cm)*	
JSL309	*mutSF30A, mutL::mutL-gfpmut2 (spc)*	
JSL311	*dnaN::dnaN-mgfpmut2 (spc), dnaX::dnaX-mCherry (cm)*	
JSL315	*ΔmutS, amyE::P_{spac}-mutSF30A-gfpmut2 (cm), dnaX::dnaX-mCherry*	
JSL328	*ΔmutS, amyE::P_{spac}-mutS800-GFP (cm)*	
JSL330	*ΔmutS, amyE::P_{spac}-mutSF30A800-GFP (cm)*	
JSL336	*ΔmutS, amyE::P_{spac}-mutS800-GFP (cm), dnaX::dnaX-mCherry (spc)*	

All strains are derivates of PY79.

Table S3. Oligonucleotides used in this study

Primer	Oligonucleotide Sequence	Restriction sites	Purpose
oJSL81	5′gcgcgcgcgtcgacatggccggttatacgcctatg	SalI	To make pJSL30
oJSL82	5′gtgggttgctcgagatgtaatttcttttgcagctt	XhoI	To make pJSL30
oJSL125	5′ggtgatgcttatgaaatgttttttgaggacg		Used to quickchange *mutS* to *mutSF30A*
oJSL126	5′cataagcatcacccaggcgaaaaaataaaaag		Used to quickchange *mutS* to *mutSF30A*
oJSL127	5′acatgcatgcttacttataaagttcgtccatgccaag	SphI	To make pJSL40
oJSL128	5′gccgctcgagatggtttcaaaaggcgaagaactg	XhoI	Used to make pJSL40
oJSL133	5′ gtgggttgctcgagcacctgaggtttctgcaccggc	XhoI	Used to make PJSL63
oJSL156	5′ gcatgcctgcaggtcgacgacagaggttgtcacagaacggg		Used to make pJSL57
oJSL157	5′ ttttgccattgtttaatccctcactatgtatcaacg		Used to make pJSL57
oJSL158	5′ gtgagggattaaacaatggcaaaagtcatccaactgtcagatgag		Used to make pJSL57
oJSL159	5′ cgacggccagtgaattccctgcttgaggaacgcgattcgg		Used to make pJSL57
oJSL168	5′ ggatcctctagagtcgacctgc		To make linear pBGSC6 for SLIC
oJSL169	5′ gaattcactggccgtcgttttacaac		To make linear pBGSC6 for SLIC
oJSL170	5′ cctgcaggtcgactctagaggatcctggggcaagcttcttgctc		To make pJSL67 with SLIC
oJSL171	5′ ttgtaaaacgacggccagtgaattcttattatttgtacagctcatccatgccac		To make pJSL67 with SLIC
oJSL178	5′ catgcagctagctaaggaggtatacatatggccggttatacgcctatg	NheI	To make pJSL58
oJSL179	5′ gatcgagcatgcttacacctgaggtttctgcaccggc	SphI	To make pJSL58

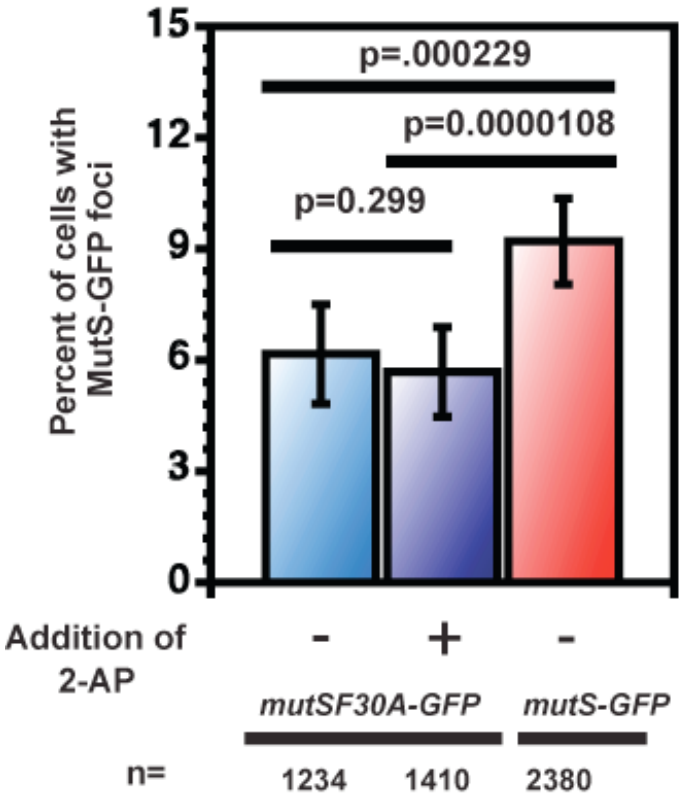

Figure S1. Response of MutS-GFP to the intrinsic error rate *in vivo.* Shown is a bar graph of the percent of cells with foci for MutSF30A-GFP with (+) and without (-) 2-AP compared to cells with MutS-GFP foci in the absence of 2-AP challenge. The p-values indicate the difference between the percent of cells with foci between each group shown. MutSF30A-GFP and MutS-GFP untreated are statistically significant. The data presented here is the same as in Figure 2C.

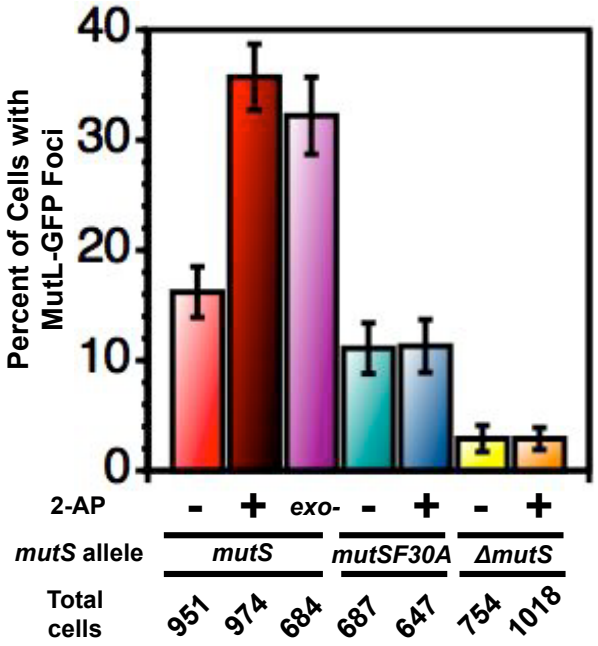

Figure S2. MutL-GFP foci formation is dependent on MutS and mismatch detection. Different *mutS* alleles were placed upstream of *mutL-gfp* to determine their effects on MutL-GFP focus formation *in vivo*. The percentage of cells with MutL-GFP foci is shown and represented as a bar graph. The number of cells for each sample scored is indicated as well as each condition. Error bars denote the 95% confidence intervals.

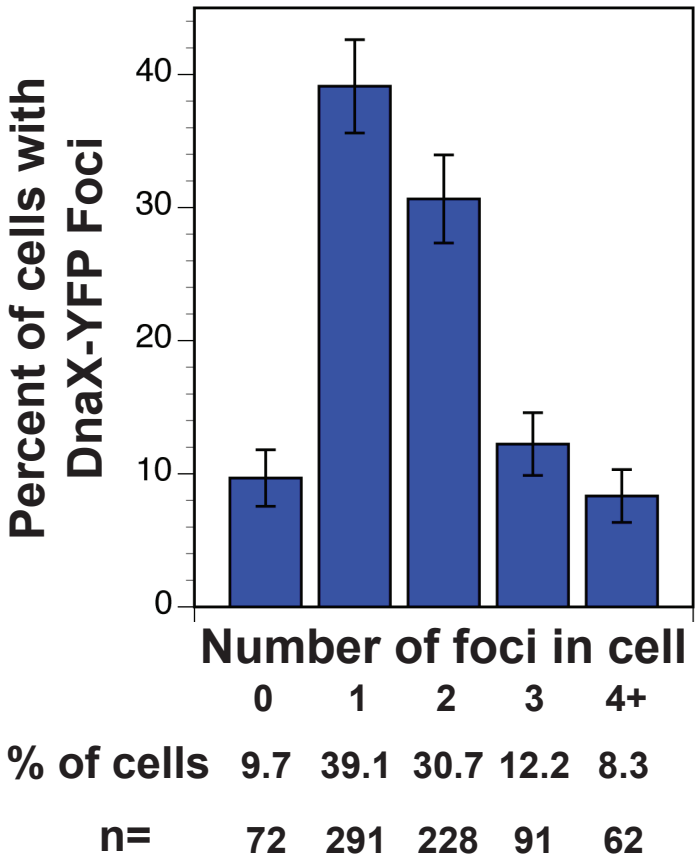

Figure S3. Scoring of DnaX-GFP foci in live cells. We scored the percentage of cells with DnaX-GFP foci in $S7_{50}$ defined minimal medium supplemented with 1% L-arabinose. The percentage of cells with 0, 1, 2, 3, and 4 or greater foci are shown. The number of cells (n) in each population are also indicated. The error bars reflect the 95% confidence interval. A total of 744 cells were scored over two independent experiments.

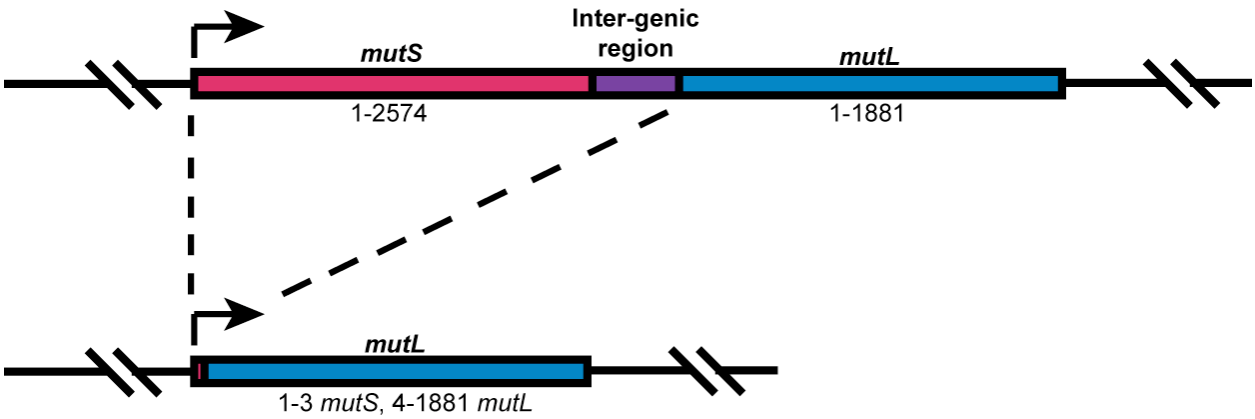

Figure S4. Schematic representation of the in frame deletion of *mutS* from the *mutSL* operon. This construct (JSL281) represents a deletion of *mutS* that maintains *mutL* under the control of its native promoter. The start codon of *mutS* (ATG) replaces the start codon of *mutL* (GTG) in order to ensure *mutL* expression. Steady state levels of MutL in this background were ~2-3 fold higher than that observed when *mutS*$^{+}$ is upstream (Fig 1D).

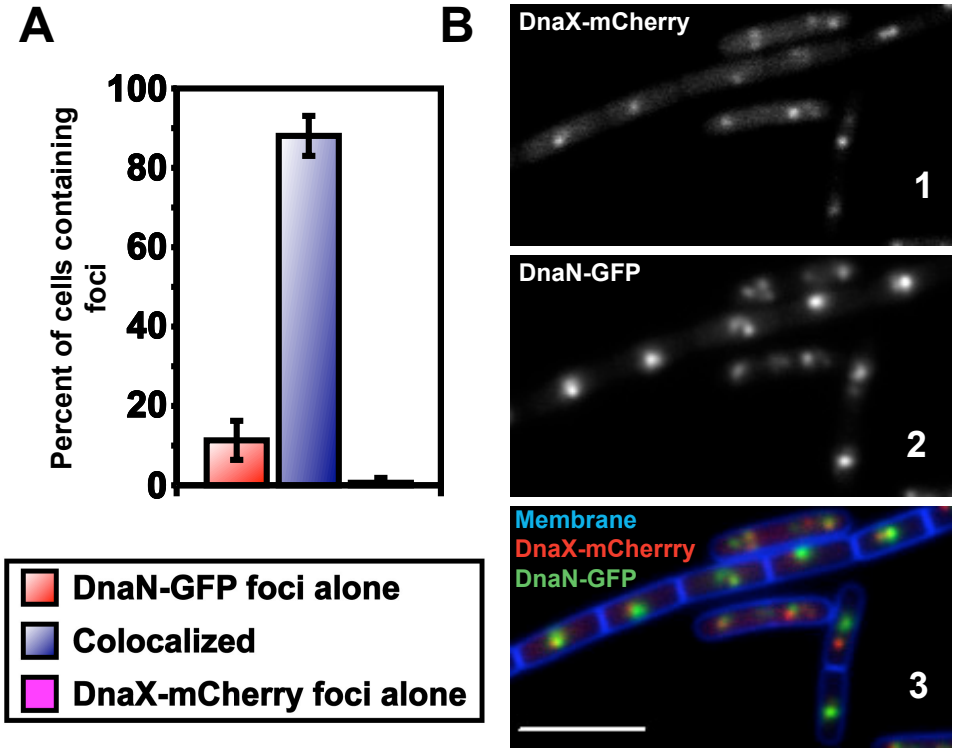

Figure S5. Colocalization of DnaX-mCherry foci with DnaN-GFP foci. (A) The bar graph shows the percentage of cells with a single replisome focus, visualized with DnaX-mCherry or DnaN-GFP. **(B)** Shown are representative images of DnaX-mCherry (1), DnaN-GFP (2), and the merge of both images with a membrane stain (3). The scale bar indicates 4 µm.

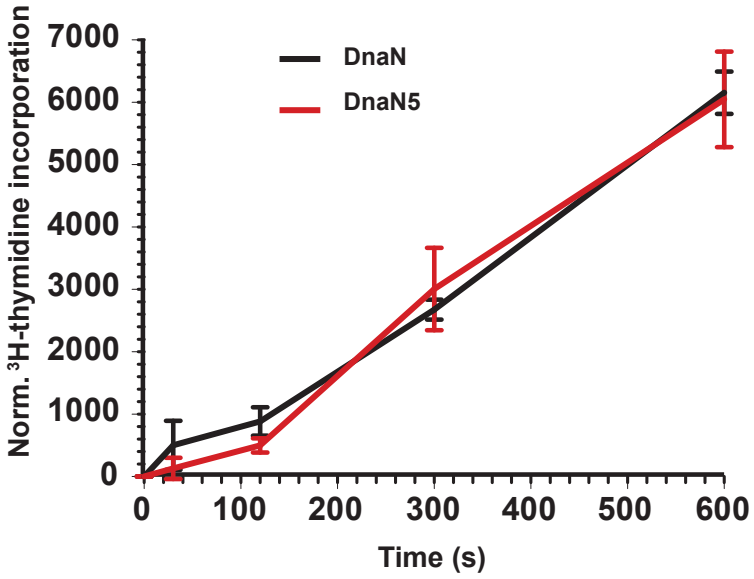

Figure S6. DnaN5 supports DNA replication to wild type levels at 37°C. The rate of DNA synthesis was measured by monitoring ^{3}H-thymidine incorporation into acid insoluble material. Each data point represents the mean of duplicate samples from 4 independent experiments. The error bars represent the standard error of the mean. ^{3}H-thymidine incorporation was normalized to OD_{600} of the samples at each time point tested.

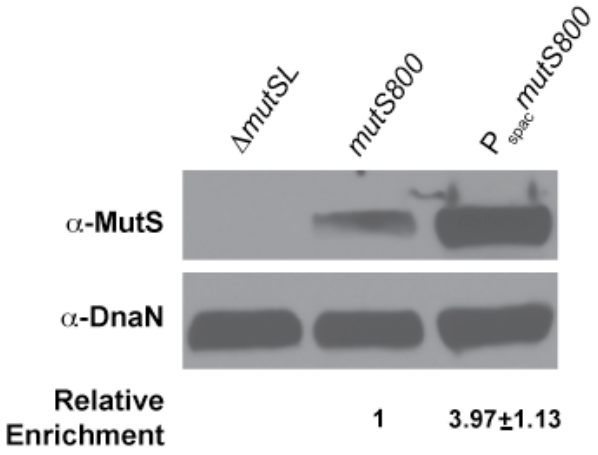

Figure S7. Quantifying ectopic expression of MutS800

Relative protein levels of MutS800 were determined by performing immunoblot analysis followed by quantification using Image J software (http://rsb.info.nih.gov/ij/). Total band intensities were determined by subtracting the background signal from the Δ*mutSL* lane followed by normalization to the total protein load determined from analysis of the DnaN band intensity. The relative enrichment was determined from 3 independent samples with the standard deviation shown.

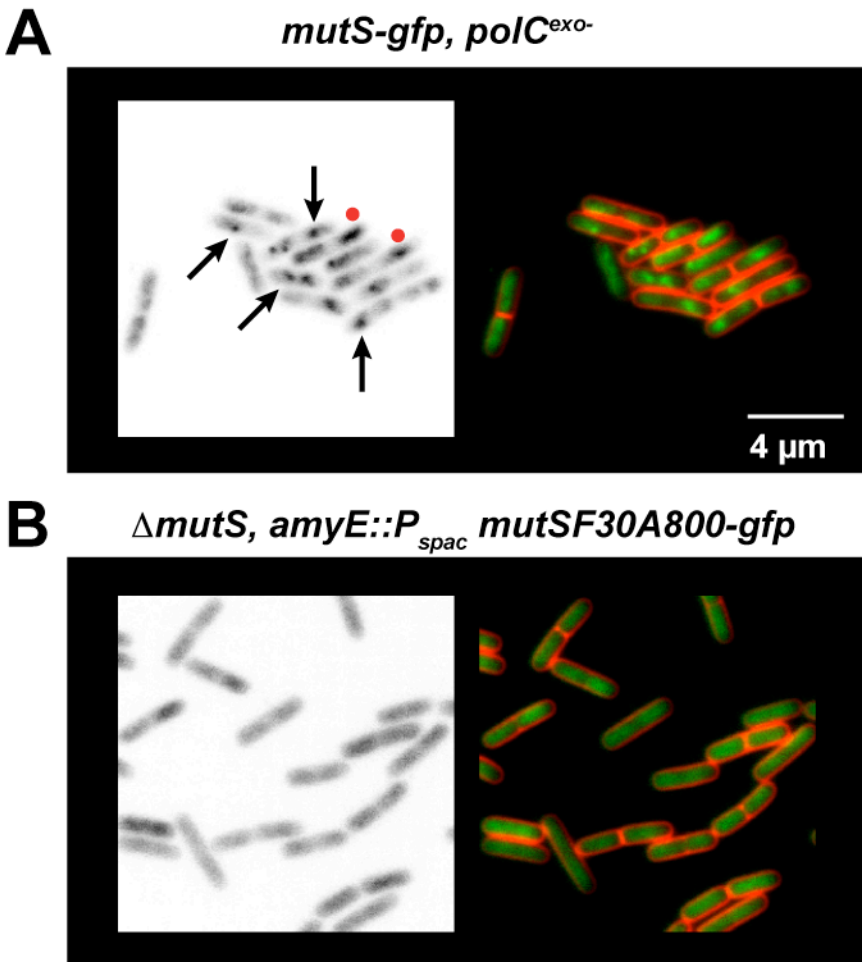

Figure S8. Method for scoring MutS-GFP foci in live *B. subtilis* cells. MutS-GFP and its derivatives form visible repair complexes *in vivo* termed foci. Repair complexes were scored as foci when visualized as having an elevated fluorescence signal occupying a discrete area above the diffuse fluorescence associated with the nucleoid. Shown in **(A)** and **(B)** are representative images of MutS-GFP or a mutant form defective in forming foci. The images are divided into an inverted monochromatic image of the GFP signal (left) and a colored image showing the GFP image in green overlaid with the membrane imaged captured with the vital membrane stain TMA-DPH (DAPI channel) and pseudo-colored red. For every experiment in this work, foci were scored using corresponding inverted monochrome images that were compared with the colored image. The average cell focus encompassed ~4% of the cell area with an average intensity 2-fold greater than background. Shown in **(A)** is a representative image of cells with MutS-GFP foci that have formed in response to natural mismatches produced by the *polC*$^{exo-}$ allele. Black arrows indicate examples of scored foci while the red circle denotes elevated nucleoid fluorescence, which does not represent MutS foci and was excluded from the

calculation. **(B)** Shown are cells with MutSF30A800-GFP, a mutant protein which fails to form repair complexes.

References

Doan, T., K. A. Marquis & D. Z. Rudner, (2005) Subcellular localization of a sporulation membrane protein is achieved through a network of interactions along and across the septum. *Mol Microbiol* 55: 1767-1781.

Dupes, N. M., B. W. Walsh, A. D. Klocko, J. S. Lenhart, H. L. Peterson, D. A. Gessert, C. E. Pavlick & L. A. Simmons, (2010) Mutations in the *Bacillus subtilis* beta clamp that separate its roles in DNA replication from mismatch repair. *J Bacteriol* 192: 3452-3463.

Hombauer, H., C. S. Campbell, C. E. Smith, A. Desai & R. D. Kolodner, (2011) Visualization of eukaryotic DNA mismatch repair reveals distinct recognition and repair intermediates. *Cell* 147: 1040-1053.

Klocko, A. D., K. M. Crafton, B. W. Walsh, J. S. Lenhart & L. A. Simmons, (2010) Imaging mismatch repair and cellular responses to DNA damage in *Bacillus subtilis*. *J Vis Exp*.

Klocko, A. D., J. W. Schroeder, B. W. Walsh, J. S. Lenhart, M. L. Evans & L. A. Simmons, (2011) Mismatch repair causes the dynamic release of an essential DNA polymerase from the replication fork. *Mol Microbiol* 82: 648-663.

Li, M. Z. & S. J. Elledge, (2007) Harnessing homologous recombination in vitro to generate recombinant DNA via SLIC. *Nat Methods* 4: 251-256.

Patrick, J. E. & D. B. Kearns, (2008) MinJ (YvjD) is a topological determinant of cell division in *Bacillus subtilis*. *Mol Microbiol* 70: 1166-1179.

Sanjanwala, B. & A. T. Ganesan, (1991) Genetic structure and domains of DNA polymerase III of Bacillus subtilis. *Mol Gen Genet* 226: 467-472.

Simmons, L. A., B. W. Davies, A. D. Grossman & G. C. Walker, (2008) Beta clamp directs localization of mismatch repair in *Bacillus subtilis*. *Mol Cell* 29: 291-301.

Smith, B. T., A. D. Grossman & G. C. Walker, (2001) Visualization of mismatch repair in bacterial cells. *Mol. Cell* 8: 1197-1206.

Sullivan, N. L., K. A. Marquis & D. Z. Rudner, (2009) Recruitment of SMC by ParB-parS organizes the origin region and promotes efficient chromosome segregation. *Cell* 137: 697-707.

Youngman, P., J. B. Perkins & R. Losick, (1984) Construction of a cloning site near one end of Tn917 into which foreign DNA may be inserted without affecting transposition in Bacillus subtilis or expression of the transposon-borne erm gene. *Plasmid* 12: 1-9.

Zheng, L., U. Baumann & J. L. Reymond, (2004) An efficient one-step site-directed and site-saturation mutagenesis protocol. *Nucleic Acids Res* 32: e115.